Pharm Res (2012) 29:2887–2901
DOI 10.1007/s11095-012-0795-4

RESEARCH PAPER

Development of a New Method to Assess Nanocrystal Dissolution Based on Light Scattering

Katharina Anhalt • Simon Geissler • Meike Harms • Markus Weigandt • Gert Fricker

Received: 09 February 2012 / Accepted: 22 May 2012 / Published online: 12 June 2012

ABSTRACT

Purpose Nanocrystals exhibit enhanced dissolution rates and can effectively increase the bioavailability of poorly water soluble drug substances. However, methods for *in vitro* characterization of dissolution are unavailable. The objective of this study was to develop an *in situ* noninvasive analytical method to measure dissolution of crystalline nanosuspensions based on light scattering.

Methods Fenofibrate nanosuspensions were prepared by wet media milling. Their solubilities and dissolution profiles in simulated gastric fluid supplemented with 0.1% Tween® 80 were measured in a small scale setup with an instrument for dynamic light scattering and the intensity of scattered light as readout parameter.

Results A good correlation was achieved between the dissolution profile of a nanosuspension measured in the light scattering setup and a conventional dissolution experiment. Nanosuspensions of 120–270 nm size could be distinguished by the light scattering method. The suspensions dissolved within 1.9–12.3 min. Over a concentration range of 40–87% of the solubility dissolution profiles of a nanosuspension with 140 nm were monitored and the determined total dissolution times were in good agreement with the Noyes-Whitney dissolution model.

Conclusions A noninvasive, sensitive and reproducible method is presented to assess nanocrystal dissolution. *In situ* measurements based on light scattering allow a straightforward experimental setup with high temporal resolution.

K. Anhalt · S. Geissler · M. Harms · M. Weigandt
Research Pharmaceutics and Drug Product Development, Merck Serono
Frankfurter Str. 250
64293 Darmstadt, Germany

K. Anhalt · M. Harms · G. Fricker (✉)
Institute of Pharmacy and Molecular Biotechnology
University of Heidelberg
Im Neuenheimer Feld 366
69120 Heidelberg, Germany
e-mail: gert.fricker@uni-hd.de

KEY WORDS dissolution · light scattering · nanocrystal · nanosuspension · Noyes-Whitney equation

INTRODUCTION

Many new drug candidates exhibit poor water solubility and thus low bioavailability after oral administration, which forms a major challenge for formulation scientists. The nanocrystal technology has emerged as a valuable tool to build the bridge between drug discovery and (pre)clinical application (1,2). Crystalline nanosuspensions are defined as colloidal aqueous dispersions of submicron sized active pharmaceutical ingredient (API) crystals and are stabilized by surfactants and polymeric steric stabilizers (2–4). The oral administration of nanosuspensions offers the advantages of enhanced bioavailability, reduced variability and diminished food effect (2–5).

The improvement in bioavailability is attributed to an enhanced dissolution rate through enlarged surface area and an increased solubility of nanocrystalline API. A high curvature, the creation of high energy surfaces and a less ordered structure of molecules in nanocrystals have been suggested to give further contributions (5). Two equations are most often quoted to provide the physico-chemical background of these phenomena. The Noyes-Whitney equation with modifications by Nernst and Brunner (6–9) describes a proportional increase in dissolution rate with increasing surface area:

$$\frac{dm}{dt} = \frac{A_0 D}{h}(C_S - C) \quad (1)$$

where dm/dt is mass rate of dissolution, A_0 is the total surface area, D is the diffusion coefficient, h is the effective

boundary layer thickness, C_S is the saturation solubility and C is the concentration of solute in the bulk solution at time t. The increase in saturation solubility is described by the Ostwald-Freundlich equation (3,10,11):

$$C_{S,r} = C_{S,\infty} \exp\left(\frac{2\gamma M}{r\rho RT}\right) \quad (2)$$

where $C_{S,r}$ is the saturation solubility of a particle with radius r, $C_{S,\infty}$ is the saturation solubility of infinitely large particle, γ is the particle medium interfacial tension, M is the compound molecular weight, ρ is the particle density, R the universal gas constant and T the absolute temperature. However, recent publications report solubility increases of not more than 15%, which is in good agreement with the Ostwald-Freundlich equation. An only small solubility increase highlights the role of an enhanced dissolution rate for the bioavailability improvement by nanocrystals (5,12).

This leads to the analytical question of determining the dissolution rate of nanoparticles, which was raised by Heng *et al.* (13), who asked "What is a suitable dissolution method for drug nanoparticles?". Basically proposed dissolution methods can be categorized as (a) being based on sampling and separation, (b) consisting of a membrane diffusion setup, or (c) true *in situ* analytical techniques.

(a) The sampling and separation technique prevails in many published studies where filtration, (ultra)centrifugation or centrifugal-filtration are used to separate undissolved nanoparticles from dissolved API (14–18). Juenemann *et al.* (19) focused on the filtration step and concluded that pore sizes of ≤0.1 μm result in predictive dissolution profiles. Shortcomings of all applied separation techniques are that they are slow and inefficient when applied to rapidly dissolving particles. It is challenging to separate particles that are less than a hundred nanometers in size, which shrink during the dissolution process. Furthermore, invasive separation steps, in which the systems to be analyzed are subjected to different forces, might alter the dissolution process. Due to the poor solubility of APIs, the dissolved concentrations are usually in the lower μg/mL range. Taking this limitation into account, it is not favorable to perform a dissolution experiment, which exposes the API to large surfaces and is therefore inevitably accompanied by adsorptive loss of API.

(b) The concept of membrane diffusion covers dialysis or reverse dialysis methods (13) and continuous flow membrane filtration under pressure (20,21). Recently, efforts have been made to modify compendial methods with dialysis membranes (USP apparatus IV (22) and USP apparatus I (23)). For studies on sustained release nanoparticulate formulations with an undissolvable matrix membrane diffusion techniques are eligible. However, results are heavily distorted for rapidly dissolving nanocrystals due to comparatively slow membrane diffusion kinetics of drug molecules.

(c) *In situ* analytical techniques, which avoid the need to separate dissolved API, are certainly the most promising approach to assess nanocrystal dissolution. Ideally, they are designed as on-line and real-time methods with high temporal resolution and have a noninvasive character. Being implemented in dissolution testing of conventional solid dosage forms it was an obvious step to use UV/VIS fiber optic probes (24–28). However, recent research disproves the use of this technique for nanosized material due to the light absorbing potential of nanoparticles (29). Moreover electrochemical analytics, like polarography, potentiometry and voltammetry, have been suggested, but are limited to electroactive APIs (30–32). Solution calorimetry has been applied to measure nanocrystal dissolution (33). Calorimetry detects many phenomena associated with any kind of molecular interaction and it is challenging to extract the net proportion of heat change resulting from particle dissolution. Nevertheless a sound method development could provide a platform for the measurement of nanoparticle dissolution by calorimetric methods in future. Finally, a turbidimetric approach to assess small particle dissolution was introduced by Tucker (34) and was followed up by Crisp *et al.* (35) and Chaubal *et al.* (36). The use of the light scattering properties of particles dispersed in liquid to monitor dissolution generated promising results and encourages further research.

In this work we focused on a light scattering technique to determine the dissolution rate as well as the solubility of crystalline nanosuspensions. The aim was to develop methods for both using an instrument for dynamic light scattering analysis, which is widespread in laboratories working on nanoparticles and is conventionally used to determine particle sizes. The light scattering properties of a cloud of particles depend on particle size and number. The correlation between scattering intensity and particle number is linear for diluted samples, in which each particle scatters light independently without being influenced by proximate particles (37,38). For variation of particle size the relation is more complex. Depending on the size range different theories describe the correlation between scattering intensity and particle size or detection angle. Larger particles scatter more light in the forward direction, whereas smaller particles scatter light isotropically (37).

The present study covers an investigation of the influence of equilibration time on the measurement of nanosuspension solubility and a solubility determination for different particle sizes. The nanosuspension dissolution by light scattering was compared to a sampling and separation

technique. Furthermore the dependance of dissolution rate on particle size and concentration gradient was investigated. Fenofibrate, a BCS class II substance was used as a poorly water soluble (<0.3 μg/mL in water, 37°C) and lipophilic (log P 5.24) model drug (39).

MATERIALS AND METHODS

Materials

Ph. Eur. grade fenofibrate (FF) was purchased from Smruthi Organics Ltd (Solapur, India), hydroxypropylmethylcellulose (HPMC) Pharmacoat® 603 from Shin-Etsu Chemical Co., Ltd. (Tokyo, Japan) and dioctyl sulfosuccinate sodium salt (DOSS) from MP Biomedicals LLC. (Solon, OH, USA). Water was of MilliQ grade (Merck Millipore, Billerica, MA, USA with 0.055 μS/cm, 5 ppb TOC). For chromatography spectroscopy grade acetonitril (LiChroSolv®, gradient grade) and trifluoroacetic acid (Uvasol®) were obtained from Merck KGaA, Darmstadt, Germany.

The dissolution medium was simulated gastric fluid (SGF) without pepsin according to United States Pharmacopeia (USP34-NF29 S1) (2.0 g sodium chloride, 80 mL 1 M hydrochloric acid in 1000 mL water) supplemented with 0.1% (w/V) polysorbate 80 (Tween® 80, Sigma-Aldrich Co. LLC., St. Louis, MO, USA). Sodium chloride and hydrochloric acid were obtained from Merck KGaA, Darmstadt, Germany in analytical grade. The pH was adjusted to 1.2±0.05. The medium was stored at 4–8°C and was used within 5 days.

Preparation of Nanosuspensions

Aqueous suspensions consisting of FF and the stabilizers HPMC and DOSS at the ratio of 20/2.5/0.1 by total suspension weight were prepared by wet media milling and stored at 4–8°C. An agitator ball mill (DynoMill Research Lab, WAB, Muttenz, Switzerland) with yttrium-stabilized zirconium oxide beads (SiLi ZY Premium 0.2–0.3 mm, Sigmund Lindner GmbH, Warmsteinbach, Germany) was used to produce nanosuspensions with particle sizes smaller than 700 nm. By variation of the process parameters milling speed (2000/3000/4000 rpm), bead fill level (50/70%) and process duration (1–120 min) distinct particle sizes could be generated.

For nanosuspensions with particle sizes bigger than 700 nm a low energy process was designed using a ball milling setup with 5 mm zirconium oxide balls (Fritsch GmbH, Idar-Obertein, Germany) agitated in a 12 mL zirconium oxide grinding bowl (Fritsch GmbH, Idar-Obertein, Germany) by magnetic stirring. For this purpose an IKA rct basic stirrer (IKA-Werke GmbH & CO.KG, Staufen, Germany) at 250 rpm and a cylindrical stirring bar 20 mm×6 mm were used. With this low energy process and with process durations of only 1 min suspensions with wide particle size distributions were obtained. To separate off larger size fractions and to create nanosuspensions of distinct particle sizes sedimentation and subsequent isolation of different supernatant layers was performed.

Light Scattering Measurements

A Zetasizer® instrument (Zetasizer Nano ZS™ with Zetasizer software 6.20, Malvern Instruments Ltd, Worcestershire, UK) was used for various purposes. The instrument and software are designed to perform dynamic light scattering (DLS) measurement for the determination of particle sizes. For this purpose light scattering intensity fluctuations are recorded and analyzed (40). In addition the instrument was used to measure absolute light scattering intensities, which can be read out as mean count rate in kilo counts per second (kcps). The mean count rate gives the arithmetic mean of the scattering signal (count rate) detected during a measurement run. The number and duration of measurement runs can be varied in the measurement settings.

The Zetasizer® instrument was equipped with a He-Ne laser (wavelength 633 nm, 4.0 mW) and an avalanche photodiode served as a detector at a detection angle of 173° (backscatter mode). In the measurement settings the attenuator and the measurement position can be varied. Since both have an influence on the intensity of scattered light it is crucial to keep them constant, when it is intended to compare absolute scattering intensities of different measurements. The incident laser light is varied by the attenuator, which can be set from 0 (total laser block) to 11 (full laser power). In this study a fixed attenuator of 10 (30% of laser light enters the sample cuvette, data provided by Malvern) was used for all determinations of absolute light scattering intensities. The measurement position was fixed at 4.65 mm (distance from cuvette wall) to ensure a constant scattering volume. The scattering volume is the area of the laser beam crossing the detection window and has a volume in the order of magnitude of 0.01 μL (data provided by Malvern). Both, attenuator and position settings, were chosen to give scattering intensity values in the range of 100–2000 kcps. All measurements were performed at 25°C in disposable semi-micro polystyrene cuvettes with lids (VWR International, LLC, Vienna, Austria).

It was validated that the laser and detector of the Zetasizer® instrument function in a constant and linear mode for the considered scattering intensities, since the instrument is calibrated for measurement and analysis of intensity fluctuations, but not for recording absolute intensity data. For that purpose the correlation between particle concentration and scattering intensity of spherical polystyrene nanoparticles (Nanosphere™ Size Standards 3150A, Z average 147±

3 nm, Thermo Fisher Scientific Inc., Waltham, MA, USA) was evaluated. The particle suspension with a concentration of 1% solids (data provided by Thermo Scientific) was diluted in 0.06% sodium chloride solution according to the dilution protocol for calibration (Malvern OQ protocol). Dilutions of $0.01–0.22\times10^{-3}$% solids were prepared and immediately the absolute scattering intensities were determined (Three measurements with 10 runs at 10 s on three independently prepared samples).

Furthermore the correlation of scattering intensity and particle concentration was explored for the suspension NS 1070 nm. Seven different dilutions in water were prepared with FF concentrations ranging from 0 to 5.5 μg/mL. The solubility was exceeded at least twofold in the prepared samples and stability of particle size throughout the measurement was assured. (Three measurements with 10 runs at 10 s on three independently prepared samples).

Particle Size Determination

Dynamic light scattering measurements were conducted for the determination of submicron particle sizes using a Zetasizer® instrument. Nanosuspensions were diluted with water to FF concentrations of typically 20–200 μg/mL. At these concentrations drug substance solubility is exceeded by at least factor twenty, which prevents particle dissolution and ensures stable particle size. The effect of nanosuspension ingredients on dispersion medium viscosity could be neglected due to the high dilutions (HPMC concentration <0.0025%). Threefold size measurements at position 4.65 mm with automated attenuator settings at 25°C were performed. The micelle size in the dissolution medium was determined respectively. Particle size is reported as intensity weighted mean hydrodynamic size (Z average) and the polydispersity index (PDI) provides a measure of distribution width.

Static light scattering (SLS) measurements were performed using a Horiba LA-950 instrument (Retsch Technology GmbH, Haan, Germany). The refractive index of FF was set to 1.51 (determined by refractive index measurements of FF solutions in ethanol and extrapolation to 0% solvent (41)). The concentration of nanosuspensions used was adjusted to meet the optimum condition of 80–90% transmission for the red laser and a 70–90% transmission for the blue laser. Size distributions measured in this manner are reported on a volume fraction basis calculated by using 15 iterations. A minimum of three repetitions was performed for each size determination.

Concentration Determination

FF concentrations were determined threefold by high performance liquid chromatography (HPLC) with UV detection at 288 nm and a reverse phase column (Zorbax Eclipse Plus C18, 4.6×50 mm, 3.5 μm, Agilent Technologies Deutschland GmbH, Boeblingen, Germany). The equipment was composed of a Merck Hitachi LaChrom L-7100 pump, a L-7360 column oven at 30°C, a L-7250 autosampler and a L-7400 UV detector. A gradient of acetonitril/water eluent acidified with 0.01% trifluoroacetic acid (V/V) was ran at a flow rate of 2 mL/min. Calibration with 1–100 μg/mL FF standards in acetonitril/water (80/20) resulted in a coefficient of determination of R^2=0.999 (mean of three independent calibration runs with freshly prepared and diluted standards)

Solubility of Drug Substance

An excess amount of FF (10 mg/mL) was dispersed in the dissolution medium and stirred for 24 h at 25±1°C. To separate off undissolved material samples were centrifuged at 16060 g for 30 min (Heraeus Biofuge fresco, Thermo Fisher Scientific Inc., Waltham, MA, USA) and subsequently the supernatant was filtered (Whatman Anotop 10 0.1 μm, GE Healthcare, Buckinghamshire, UK). Control DLS measurements were performed on the filtrates and absence of undissolved material was assumed if no particles apart from polysorbate micelles could be detected. The concentration of dissolved drug was quantified by HPLC. Three independent experimental series with triplicates were performed and the arithmetic means and standard deviations are reported.

Solubility of Nanosuspensions by Light Scattering

To determine the solubility of nanosuspensions an approach of monitoring the presence of solid nanoparticles by light scattering (instead of determining concentrations of dissolved material) was introduced by Lindors *et al.* (42) and taken up by van Eerdenbrugh *et al.* (5). In the presented study this method was modified by using a Zetasizer® instrument to measure the scattering intensity.

At the time zero nanosuspension dilutions of 0–14 μg/mL FF in dissolution medium were prepared and stored at 25±1°C. At distinct time points the samples were homogenized via shaking and absolute scattering intensities were measured (one measurement with 8 runs at 8 s). The resulting data were plotted in a scattering intensity *vs* concentration graph and two linear segments could be identified: The first one represents completely dissolved samples with scattering intensities equal to blank medium and the second one represents partially dissolved samples with a slope corresponding to an increasing solid fraction. To a minimum of seven data points of each branch a linear function was fitted. Their intersection point was calculated and interpreted as the nanosuspension solubility. For all dilutions the concentration of the nanosuspension excipient DOSS was

below the critical micelle concentration (43) and hence it was avoided that solubilization influences solubility. Each experiment was performed in triplicate and arithmetic means and standard deviations are reported.

Nanosuspension Dissolution by Light Scattering

Nanocrystal dissolution was followed by monitoring changes of light scattering intensities with a Zetasizer® instrument. The dissolution experiments were conducted at concentrations below the nanosuspension solubility after 24 h (S_{NS24h}) and nanosuspensions were diluted with the dissolution medium (SGF supplemented with 0.1% of polysorbate 80) in two steps. In the predilution step 1–10 µL of nanosuspension were added to 5–10 mL of medium under magnetic stirring to a concentration 8–10 fold above the solubility S_{NS24h}. Within 30 s the final dilution step was performed directly in the cuvette by adding 20–100 µL of prediluted nanosuspension to a total volume of 1 mL and this time was defined as zero. Gentle mixing was performed by four 180°-turnings of the cuvette taking care of no air bubbles to occur. A series of measurements was started subsequent to placing the cuvette in the sample cell. Measurement parameters were: 2 runs at 2 s, measurement position 4.65 mm, attenuator 10 and 25°C. Before each dissolution experiment a blank medium measurement was conducted in the identical cuvette already containing the respective volume of medium for the final dilution step. The final result is reported as Δ Mean Count Rate, which is the mean count rate of each dissolution measurement reduced by the mean count rate of the blank measurement.

Data Evaluation of Dissolution Experiments

Exponential models were chosen to describe the dissolution curves in an empirical and pragmatic way and to enable the calculation of characteristic data points to improve the comparability of different dissolution profiles. Selection of functions for data fitting was governed by the intention of introducing only a low level of complexity. Exponential (Eq. 3) and biexponential (Eq. 4) functions have been described to model dissolution data previously (9,44,45) and especially biexponential models have been successfully fitted to dissolution profiles of micron and submicron particle size distributions (26,28,46,47). Since in this study simple exponential function fitting was not sufficient in all cases, biexponential function fitting was applied for all tests.

$$\mathrm{ExpDec1}: f(t) = Me^{(-t/c)} + y_0 \tag{3}$$

$$\mathrm{ExpDec2}: f(t) = M_1e^{(-t/c_1)} + M_2e^{(-t/c_2)} + y_0 \tag{4}$$

f(t) is the scattering intensity (Δ Mean Count Rate) in kcps, t is the time after dilution in minutes and M, c and y_0 are the unknown function parameters. To compare the goodness of fit to both models not the coefficient of determination R^2, but the adjusted coefficient of determination $R^2_{adjusted}$ was chosen. $R^2_{adjusted}$ is more meaningful, when comparing models with different numbers of parameters (see (6) for calculation of $R^2_{adjusted}$).

The fitted functions were further analyzed by calculating the time, when only 1% of the initial scattering intensity (fitted parameter M or M_1+M_2) remains. This time is defined as the total dissolution time DT

$$\mathrm{ExpDec1}: f(DT) = 0.01M \tag{5}$$

$$\mathrm{ExpDec2}: f(DT) = 0.01(M_1 + M_2) \tag{6}$$

By applying these equations the function offset y_0 was neglected. This was possible, since y_0 was very small compared to M or M_1+M_2, respectively (<10 kcps). The function fitting and determination of DT was performed for each repetition of a dissolution experiment. Subsequently arithmetic means and standard deviations of DT were calculated.

Nanosuspension Dissolution by Conventional Method: Dilution-Sampling-Separation

A dissolution test with NS 1070 nm in a USP II paddle apparatus (DT 80, Erweka GmbH, Heusenstamm, Germany) at 25±1°C and 100 rpm rotation speed was performed. NS 1070 nm was added to 500 mL dissolution medium to a FF concentration of 5.5 µg/mL. After 2.5 min, 5 min, 10 min, 15 min, 20 min, 30 min, 45 min, 60 min, 90 min and 120 min 1 mL samples were withdrawn and filtered through a 0.02 µm syringe filter (Whatman Anotop 10). The first 0.5 mL of filtrate was discarded. The filtrate was analyzed for undissolved material by a DLS measurement. Absence of drug crystals was assumed, if no particles apart from polysorbate 80 micelles could be detected. Concentrations of the filtrates were determined by HPLC and represent the dissolved concentration. The undissolved fraction was calculated by subtraction of the dissolved concentration from the total drug concentration.

RESULTS

Characterization of Suspensions and Dissolution Medium

Table I reports the particle sizes of nanosuspensions. Stability of particle size and distribution was monitored and

Table I Partice Size (diameter [nm]) and Particle Size Distributions of Suspensions Measured by SLS and DLS, $n=6$

	SLS				DLS	
	Mean	D10	D50	D90	Z average	PDI
NS 120 nm	123 ± 4	72 ± 1	113 ± 3	188 ± 7	219 ± 2	0.204 ± 0.005
NS 140 nm	138 ± 2	79 ± 1	130 ± 2	210 ± 4	215 ± 4	0.184 ± 0.013
NS 160 nm	156 ± 12	80 ± 2	138 ± 5	237 ± 13	280 ± 5	0.189 ± 0.024
NS 180 nm	184 ± 5	92 ± 2	168 ± 5	293 ± 9	296 ± 3	0.183 ± 0.021
NS 270 nm	266 ± 3	97 ± 1	193 ± 3	501 ± 10	381 ± 10	0.265 ± 0.041
NS 650 nm	645 ± 79	142 ± 29	365 ± 89	1491 ± 100	618 ± 25	0.207 ± 0.036
NS 800 nm	797 ± 109	155 ± 64	647 ± 214	1630 ± 53	714 ± 79	0.566 ± 0.444
NS 1070 nm	1068 ± 44	247 ± 40	918 ± 42	2099 ± 73	–	–

ascertained for a minimum of 4 weeks. The crystalline state of the suspended nanoparticles was verified previously (data not shown).

The dissolution medium was characterized by DLS measurements on eight batches. The size of polysorbate 80 (Tween® 80) micelles was 10.6 ± 0.9 nm with a polydispersity index of 0.112 ± 0.040. Blank medium measurements for dissolution experiments gave scattering intensities of 82 ± 5 kcps.

Validation of Linearity of Light Scattering Measurements

For the spherical polystyrene nanoparticles a linear correlation between particle concentration and scattering intensity prevailed in the range of 100–2000 kcps (R^2=0.997). This linear correlation is in accordance with theory (37,38) and consequently this experiment can serve as a proof for linear functionality of the laser and detector for the considered instrument settings and measured scattering intensities. For higher particle concentrations and therefore higher scattering intensities a deviation from linearity was observed. In the second experiment the investigation of dependance of scattering intensity on concentration was extended to the suspension NS 1070 nm. In contrast to the Nanosphere™ Size Standard this system is polydisperse with particles in the nano- to micrometer range and particle shape deviates from ideal sphericity. Nevertheless a linear correlation of scattering intensity and particle concentration was observed (R^2=0.998).

Solubility

All solubility results are summarized in Table II and Fig. 1 presents the scattering intensity *vs* concentration graphs for the determination of nanosuspension solubilities. For the linear function fitting data points below 8 μg/mL and above 10.5 μg/mL were taken into account. Points near to the solubility limit were excluded due to a higher uncertainty of data interpretation (5). For the horizontal branch coefficients of correlation are low, which can be explained by a low signal-to-noise ratio for the measured scattering intensities of 75–90 kcps. Nevertheless this does not alter the data analysis essentially, since both branches can be clearly distinguished regarding slope and intercept.

A first set of experiments was conducted with NS 140 nm and a variation of time (Fig. 1a). The aim was to identify the time necessary to reach an equilibrated system (stable dissolved and solid concentration over time) for the determination of equilibrium solubility. The 0 h-graph shows the scattering data recorded 10 s after dilution and it exhibits a curved shape. However, for stable particles a linear increase of scattering intensity with increasing particle concentration would be expected. The deviation from linearity indicates that particles are not stable and that the particle dissolution process has already started. After 2 h the two-branched shape becomes visible, in which the horizontal branch corresponds to completely dissolved samples and the rising branch to partially dissolved samples. After 24 h the picture is the same with a shift to higher concentrations. After 96 h the rising branch flattens and it is not possible to clearly identify a linear progression due to signal fluctuations.

It was not possible to identify the time to reach a completely equilibrated system, in which the solubility would correspond to saturation solubility. Data interpretation from the 96 h-graph is subject to statistical shortcomings: The fluctuations of the scattering signal can be explained by number fluctuations in the scattering volume. The term number fluctuation describes the effect of a very low number of particles in the scattering volume, which results in poor statistical validity of the measurement. Data interpretation of the 96 h-graph is further challenged by possible changes in particle size distribution and therefore light scattering properties of the system, since not only dissolution, but also aggregation or Ostwald ripening might have been occurred. Furthermore, adsorption of API or particles onto

Table II Solubility of FF Drug Substance (S_{FF}) and of Nanosuspensions (S_{NS})

		Scattering method: Linear function fitting					Solubilty S_{NS}	
Nanosuspension	time [h]		Data Points n	Slope [kcps/μg/mL]	Intercept [kcps]	R^2	Intersection Point [μg/ml]	Relative Solubility [% S_{FF}]
NS 140 nm	2	dissolved	9	0.9	82.9	0.752	9.57 ± 0.17	110.1 ± 9.1
		undissolved	7	365.8	−3408.4	0.995		
	24	dissolved	7	1.0	77.5	0.910	9.86 ± 0.02	113.4 ± 9.0
		undissolved	15	246.4	−2340.8	0.994		
	96	dissolved	7	1.1	88.7	0.683	10.38 ± 0.01	119.5 ± 9.0
		undissolved	15	32.7	−239.7	0.751		
NS 270 nm	24	dissolved	7	1.0	76.2	0.661	8.70 ± 0.24	100.1 ± 9.4
		undissolved	15	276.2	−2318.4	0.992		
NS 1070 nm	24	dissolved	7	0.4	78.3	0.392	9.62 ± 0.50	110.7 ± 10.4
		undissolved	15	129.3	−1162.5	0.964		
Drug substance							Solubilty S_{FF}	
FF	24	Conventional solubility determination method					8.69 ± 0.78	100.0 ± 12.7

the plastic cuvettes might be a potential source of error and might be responsible for the shift of scattering graphs towards higher concentrations for longer equilibration times.

As a conclusion of the described results, the equilibration time of 24 h was selected for further experiments, because on the one hand the particle dissolution process is in an advanced state and on the other hand data interpretation is still possible with adequate statistical quality. Following the definitions given by Sugano the measured solubilities (S_{NS24h}) are apparent solubilities, meaning that reasonable long incubations times were chosen without the confirmation of stable dissolved and solid concentration over time (48).

Figure 1b presents the second set of experiments, in which the particle size was varied using NS 140 nm, NS 270 nm and NS 1070 nm. For NS 270 nm a significantly lower solubility S_{NS24h} was determined than for the smaller NS 140 nm (8.70 ± 0.24 *vs* 9.86 ± 0.02 μg/mL). This finding is consistent with the Ostwald-Freundlich equation (Eq. 2) in terms of an expected higher solubility for the smaller sized nanosuspension. However, the solubility S_{NS24h} of NS 1070 nm was calculated to be 9.62 ± 0.50 μg/mL and hence higher than for the suspensions NS 270 nm with smaller particle size. This result can be interpreted as a lack of suitability of the scattering method for NS 1070 nm, which is due to its lower particle number density (number of particles per volume). At concentrations just above the solubility limit only few undissolved particles remain, which are not detectable with the optical configuration of the Zetasizer®. This provokes the misleading interpretation of these samples as dissolved, where there might indeed be particles left. It consequently leads to an overestimation of solubility. Another effect, which amplifies the shortcomings of the

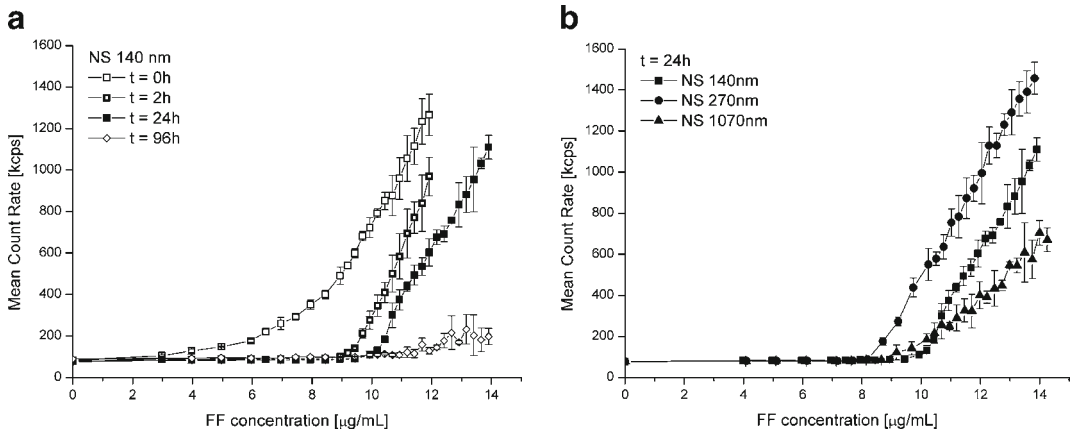

Fig. 1 Solubility of nanosuspensions determined by light scattering method. Measured scattering intensity *vs* total FF concentration. (**a**) Solubility of NS 140 nm after equilibration times of 0 h, 2 h, 24 h and 96 h. (**b**) Solubility (S_{NS24h}) of nanosuspensions with different particle sizes after 24 h. *n*=3, arithmetic mean±standard deviation.

scattering method for this suspension, is that smaller particles dissolve preferentially and the size distribution is altered towards bigger particles, that are more difficult to be detected (5). Furthermore, instabilities like aggregation and Ostwald ripening can also lead to larger particles and thus increase the error. Even though samples are shaken up directly before each measurement, settling of particles during the measurement might contribute to the high standard deviations as well.

Unlike in previous publications (5,42) all dilutions were prepared in one step and were not gradually increased by stepwise addition of suspensions to the cuvette. This approach was chosen to be in close analogy to the standard procedure, in which an excess drug amount is added at the beginning. Due to preferential dissolution of smaller size fractions and Ostwald ripening, a one step dilution might lead to different size distributions and scattering properties among the samples and could influence results. We demonstrated that this effect was not relevant for the determination of solubilities of the smaller sized suspensions. Linearity of the ascending branch and reasonable results confirm the suitability of the presented method. However, a gradual increase of concentration might improve the suitability of the method for the determination of bigger sizes suspensions (like for example NS 1070 nm).

The experimental error of the solubility determination by light scattering is small compared to the uncertainty of the drug substance solubility determination (Table II). Relative standard deviations of S_{NS24h} for NS 140 nm and 270 nm are 0.3% and 2.8% compared to 9.0% for the drug substance solubility S_{FF}. Therefore, most of the variability in the calculated relative solubilities (S_{NS24h}/S_{FF}) originates from S_{FF}. This highlights the potential of the proposed method to determine relevant solubility differences of nanocrystal formulations with good precision.

Dissolution by Light Scattering

The measurement of nanocrystal dissolution by an approach of monitoring decreasing solid particle number and size based on light scattering proved to provide a very fast data acquisition. The first data point was recorded 25 s after dilution and the interval of subsequent data points was 10 s. The scattering intensity, which is the primary measurement signal of each DLS measurement, was considered as readout parameter. The standard data output of DLS measurements, the hydrodynamic particle diameter, is derived from the intensity fluctuations by complex data analysis and exhibits a poor statistical quality for the extremely short measurement time of 2 s applied within this work (40).

In the following the light scattering dissolution method will be compared to the conventional dissolution method. Subsequently the applicability of the new method will be demonstrated. For that purpose two sets of experiments were carried out to investigate suitability, reproducibility and sensitivity. In a first step the particle size was varied at a constant concentration; in a second step the concentration was varied keeping the particle size constant.

Comparison of Light Scattering Dissolution Method and Conventional Method

For the nanosuspension NS 1070 nm a direct comparison of both techniques was made (Fig. 2). An overlay of both dissolution diagrams was designed by plotting the undissolved concentration determined by conventional paddle dissolution and the recorded scattering intensity determined by the scattering method. The resulting dissolution curves share the first data point at 2.5 min and the last data point at 120 min. The Y-axes were scaled so that the diagrams overlap at 2.5 min and 120 min. The values at time point 0 min could not be used to adjust the scales, because it was not possible to measure the scattering intensity at time 0 min.

The overlay illustrates a good correlation of both techniques. Especially the initial high dissolution rate (0–10 min) is correlated very well. In the middle part (10–60 min) the dissolution process is slowed down and the scattering result has a decreasing tendency with many spikes. In the conventional experiment 92% are dissolved after 60 min and the dissolution curve slowly approaches the level of complete dissolution. In the scattering result this process is indicated by a continuous reduction in the number of intensity spikes. The fluctuations of the scattering signal and the intensity spikes can be explained by number fluctuations in the scattering volume. Due to the small scattering volume and the decrease in particle concentration, when the dissolution process reaches its end, the probability of remaining particles to be detected is low. The spikes represent remaining undissolved particles passing the scattering volume, which probably belong to micron sized particle fractions. To optimize the comparability of both dissolution graphs a further step of data analysis was performed on the scattering diagram. The scattering intensity data were smoothed by the running mean algorithm with 75 data points.

Analysis of the dissolution graphs by (bi-)exponential function fitting and calculation of DT shows a very good fit of the biexponential model to the conventional dissolution graph ($R^2_{adjusted}=0.995$ compared to $R^2_{adjusted}=0.930$ for exponential model). The corresponding dissolution times are calculated to be 76 ± 21 min for the scattering method and 132 ± 8 min for the conventional method (see Table III). A shorter dissolution time was derived from the scattering method as from the conventional method. This discrepancy is probably attributed to an inappropriate representation of the intensity spikes at

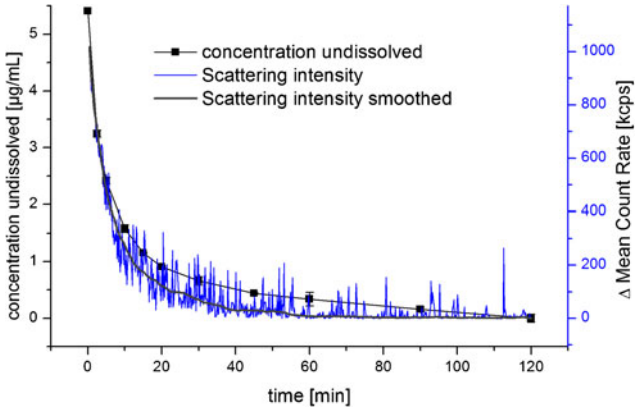

Fig. 2 The dissolution of NS 1070 nm in simulated gastric fluid supplemented with 0.1% polysorbate 80 at a FF concentration of 5.5 µg/mL. Black line: conventional method, $n=3$, arithmetic mean±standard deviation. Blue line: light scattering method, $n=6$, arithmetic mean, standard deviations not shown for clarity reasons. Grey line: smoothed light scattering signal (running mean, 75 data points).

advanced dissolution state by the applied evaluation method. It is expected that the scattering method is more suitable for the smoother dissolution profiles of smaller particles (Fig. 3) and more appropriate dissolution times are calculated.

Nanocrystal Dissolution by Light Scattering Method

Compared to the conventional method, in which dissolved concentrations are measured quantitatively, the light scattering setup primarily provides relative dissolution profiles. When the scattering intensity approaches a constant level, it can be concluded that the number and size of particles are at a constant level, but information about the amount of undissolved drug cannot be derived directly. In this study for all samples at the end of the dissolution process a Δ Mean Count Rate of 0±10 kcps was reached (Figs. 3 and 4), indicating that light was only scattered by the dissolution medium itself and not by nanocrystals. A DLS size measurement at the end of the process confirmed that apart from micelles no particles were detectable. Therefore it was possible to add quantitative information regarding the end of the process.

Figure 3 presents the experimental dissolution curves for NS 120 nm to NS 270 nm. From the Noyes-Whitney equation (Eq. 1) it is predicted that the smaller nanosuspensions with their higher surface area exhibit higher dissolution rates and therefore shorter dissolution times. In Fig. 3 this dissolution time *vs* particle size ranking can be seen. For the sake of clarity results for bigger sized suspensions NS 650 nm to NS 1070 nm are not included in Fig. 3. However, Fig. 2 shows the dissolution curve of NS 1070 nm and Table III gives the determined dissolution times for all formulations. The slower dissolution rates of NS 650 nm to NS 1070 nm can be explained by micron sized particle fractions present in this formulations (D90 > 1 µm, Table I).

Figure 4 presents the experimentally obtained dissolution curves for different particle concentrations. For steeper concentration gradients higher dissolution rates and therefore shorter dissolution times are observed, which corresponds to the ranking as expected from the Noyes-Whitney equation. In pharmaceutical dissolution testing it is favored to minimize the concentration gradient effect by choosing sink conditions, which means that the total drug concentration C_0 is less than 10–30% of saturation solubility C_S (49,50). For sink conditions the decrease in concentration gradient with increasing dissolved concentration can be neglected and the process can

Table III Fitting of Exponential (ExpDec1) and Biexponential (ExpDec2) Functions to Dissolution Curves and Calculation of Dissolution Time (DT)

		ExpDec 1 fitting		ExpDec 2 fitting	
		$R^2_{adjusted}$	DT [min]	$R^2_{adjusted}$	DT [min]
Scattering method: Var. concentration	3.9 µg/mL	0.975	1.52±0.43	0.985	1.69±0.30
	4.7 µg/mL	0.976	1.79±0.32	0.981	2.15±0.38
	5.5 µg/mL	0.983	2.19±0.49	0.990	2.93±1.06
	6.9 µg/mL	0.968	3.14±0.28	0.977	3.44±1.02
	8.6 µg/mL	0.932	5.11±0.69	0.943	6.84±0.57
Scattering method: Var. size	NS 120 nm	0.990	1.56±0.14	0.993	1.89±0.33
	NS 140 nm	0.983	2.19±0.49	0.990	2.93±1.06
	NS 160 nm	0.978	3.30±0.29	0.984	4.70±0.95
	NS 180 nm	0.987	6.29±0.37	0.995	7.05±0.73
	NS 270 nm	0.969	10.52±0.63	0.974	12.25±0.34
	NS 650 nm	0.827	15.32±3.59	0.861	18.17±1.22
	NS 800 nm	0.675	31.03±5.37	0.698	60.25±11.76
	NS 1070 nm	0.600	36.62±6.18	0.623	76.36±21.16
Conventional method	NS 1070 nm	0.930	43.30±0.95	0.995	132.24±8.36

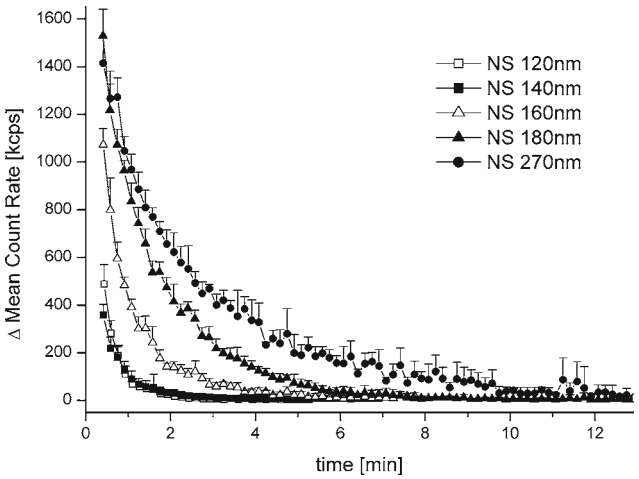

Fig. 3 Nanosuspension dissolution measured by light scattering. Variation of particle size at a fixed FF concentration of 5.5 μg/mL. *n*=4, arithmetic mean+standard deviation.

be regarded as only dependent on the constant C_S. However, in the presented experiment concentrations above 30% of apparent nanosuspension solubility (S_{NS24h}) are analyzed. Due to the rapid process of nanocrystal dissolution, too few data points for dissolution under sink conditions were obtained for a satisfying data interpretation.

Table III summarizes the results of the fitting of (bi-)exponential models to experimental dissolution graphs and the calculated dissolution times. In general the tendency for a slightly better fit of ExpDec2 (Eq. 4) was observed. The function fitting to dissolution curves of bigger sized suspensions (NS 650 nm–NS 1070 nm) and of higher concentrations (8.6 μg/mL) resulted in lower coefficients of determination. However, this should not necessarily be interpreted as a poor correlation, since the relatively high noise of these dissolution curves (see Fig. 2, blue line) inevitably results in high deviations between the measured signal and the fitted curve.

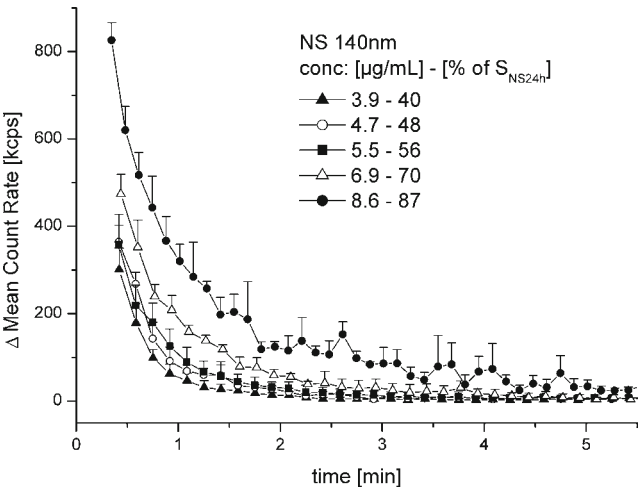

Fig. 4 Nanoparticle dissolution measured by light scattering. Variation of total FF concentrations for NS 140 nm. Concentrations are given in μg/mL and as fraction of the apparent solubility S_{NS24h} of NS 140 nm. *n*=4, arithmetic mean+standard deviation.

Investigation of Experimentally Obtained Results According to the Noyes-Whitney Equation

The Noyes-Whitney dissolution model describes the dissolution process as being determined by diffusion of dissolved molecules through the diffusion layer adjacent to the solid surface. In strict interpretation its validity is limited to a constant surface area, a bulk concentration being considerably lower than the solubility of the API and to surfactant free dissolution media. In practice the Noyes-Whitney model has been successfully applied to dissolution experiments, which did not meet all of the above mentioned criteria (46,51,52). This indicates the usefulness of the model even under non perfect conditions and motivated the use of the Noyes-Whitney equation as a first approach in this study. For that purpose the Hixson and Crowell equation was used, which is a transformation of the Noyes-Whitney equation (Eq. 1) (9).

$$W_d = VC_S\left(1 - e^{-Kt}\right) \tag{7}$$

W_d is the mass dissolved, C_S the saturation solubility, V the volume of dissolution medium, t the time and coefficient K is

$$K = \frac{DA_0}{hV} \tag{8}$$

The total initial surface area A_0 of the suspensions is estimated with following assumptions: (1) Particles have a spherical shape and the radius r. (2) Particle size distributions are neglected. (3) Due to the extremely poor solubility of FF it is neglected that the aqueous medium is saturated with dissolved FF. All drug substance is considered to be in the solid nanocrystalline state. (4) The density ρ of crystalline fenofibrate is 1.177 g/cm³ (predicted value by I-Lab 2.0 software, ACD/Labs, Toronto, Canada). As an approximation the shrinking of particles and the change of surface area during the dissolution process were not taken into account.

$$A_0 = N^* A_P = \frac{V_0{}^* A_p}{V_P} = \frac{W_0}{\rho}\frac{3}{r} \tag{9}$$

N represents the number of particles, V_0 and W_0 the total volume and mass of particles and V_P and A_P the volume and surface area of an individual particle.

Equation 7 is transformed by applying logarithms and by substituting $W_S = VC_S$ and $W_d = W_0\text{-}W_u$ (W_0 is the total drug amount and W_u is the undissolved drug mass):

$$\ln\frac{(W_u + (W_S - W_0))}{W_S} = -Kt \tag{10}$$

W_S-W_0 is the gradient ΔW. The time, when dissolution terminates DT is characterized by W_u=0. The total drug concentration is C_0 (=W_0/V). Equations 11 and 12 can be obtained by transformation of Eq. 10 and insertion of Eqs. 8–9:

$$DT = -\ln\frac{\Delta W}{W_S}\frac{1}{K} = -\ln\frac{W_S - W_0}{W_S}\frac{hV}{DA_0} = -\ln\frac{C_S - C_0}{C_S} * \frac{h\rho r}{3DC_0} \quad (11)$$

$$-\ln\frac{\Delta W}{W_S}\frac{V}{A_0} = k^*DT \quad (12)$$

Equation 12 denotes that the -ln(ΔW/W_S)*V/A_0 *vs* DT diagram has a slope of k = D/h, where k is the dissolution rate constant and where the y-intercept is zero. Figure 5 shows the DT *vs* -ln(ΔW/W_S)*V/A_0 diagram for the dissolution of NS140 nm at different concentrations and the result of linear regression. From the reciprocal slope a dissolution rate constant of 9.4*10^{-4} cm/s is derived. For the experimental data an offset was observed, thus for the linear regression analysis the y-intercept was not forced to be zero (see Discussion, "Investigation of Experimentally Obtained Results According to the Noyes-Whitney Equation").

For the analysis of dissolution with varying particle sizes differences in the saturation solubility C_S were not considered, since their contribution to the term -ln(ΔW/W_S)*V/A_0 is small compared to the contribution of particle size. Instead as an approximation the value of S_{NS24h} for NS 140 nm was assumed for all calculations. Figure 6 shows the DT *vs* -ln(ΔW/W_S)*V/A_0 diagram for the dissolution of different formulations at a constant concentration and the result of linear regression. From the reciprocal slope a dissolution rate constant of 5.1*10^{-4} cm/s is derived, which is in a similar range as determined by variation of concentration.

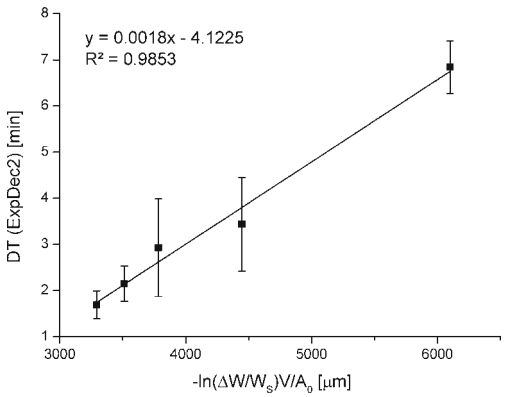

Fig. 5 Plot of dissolution times (DT) *vs* -ln(ΔW/WS)*V/A_0. Dissolution times were experimentally determined by light scattering dissolution method with NS 140 nm at different concentrations (40–87% of saturation level). For the calculation of the total surface area A_0 the particle radius of 65 nm (D50) was applied.

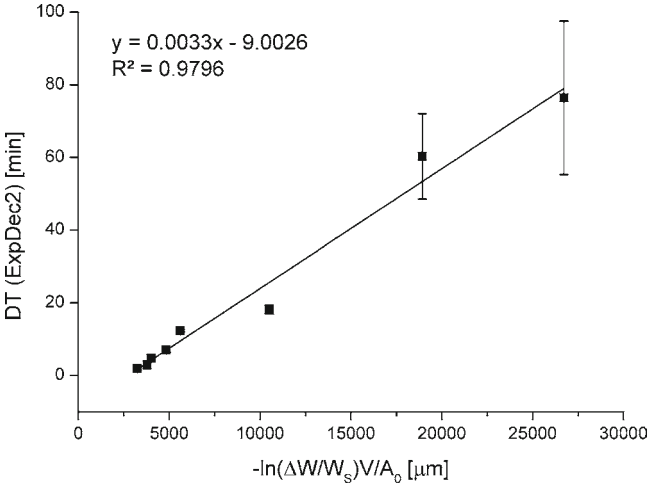

Fig. 6 Plot of dissolution times (DT) *vs* -ln(ΔW/WS)*V/A_0. Dissolution times were experimentally determined by light scattering dissolution method with nanosuspensions of different particle sizes at a concentration of 5.5 μg/mL. For the calculation of the total surface area A_0 particle radii measured as D50 were applied.

DISCUSSION

Solubility of Nanocrystals

The light scattering based determination of nanosuspension solubility proved to be a reproducible, sensitive and experimentally convenient approach. The suitability of the Zetasizer® instrument for this application was demonstrated. The advantages over separation based techniques and the good agreement of measured with estimated solubilities based on the Ostwald-Freundlich equation were summarized by van Eerdenbrugh (5). Limitations of the applied method became apparent for samples with mainly micron sized particles. Their reduced particle number density and the sedimentation tendency of microparticles negatively affect data quality. Previously relative solubilities of 114.5±2.1% for a itraconazole nanosuspension (Z average 220±4 nm), 106.7±1.0% for a phenytoin nanosuspension (Z average 406±17 nm) and 97.0 ±1.4% for a naproxen nanosuspension (Z average 288± 4 nm) have been reported (5). We determined relative solubilities of 113.4±9.0% for NS 140 nm (Z average 215±4 nm) and of 100.1±9.4% for NS 270 nm (Z average 381±10 nm). These results are in accordance with published and theoretically predicted values (5,12) and hence confirm the adequacy of the proposed method to determine nanocrystal solubility.

Previous investigators (5,42) focused on solubility increase but not on the kinetic nature of the dissolution process. From the findings of the experiment in this study dealing with time variations (Fig. 1a) the importance of the time factor becomes obvious. The nanocrystal dissolution experiments can be regarded as a consistent continuation of the solubility experiments with a shift of the timescale from hours to minutes.

Nanocrystal Dissolution by Light Scattering Method

Conventional dissolution techniques often follow the principle of dilution, sampling, separation and quantification of dissolved material. The alternative approach presented here probes the presence of nanoparticles by light scattering. It can be described as a straightforward dilution and *in situ*-measurement technique. All sampling, separation and chromatographic quantification steps are avoided. The elimination of the separation step is especially favorable for nanocrystal dissolution due to its inefficiency, slowness and invasive character. A continuous and fast data acquisition offers a much higher information density as can be achieved with the conventional method. An additional feature of the presented method is its small scale setup. By operating with a nanosuspension volume of a few μL, dissolution experiments could easily be integrated in early formulation development studies with typically limited availability of API. In a direct comparison a light scattering dissolution experiment matched a conventionally generated dissolution curve remarkably well, which demonstrates the eligibility of the alternative technique.

In this study a linear correlation of scattering signal and particle concentration was shown exemplarily (see Results, "Validation of Linearity of Light Scattering Measurements"). This allowed the simplified assumption that during dissolution decreasing scattering intensity corresponds to decreasing particle concentration. However, scattering depends not only on particle concentration, but also on size. To deal with the effect of differences in scattering patterns of different sized nanocrystal formulations the comparison of their dissolution profiles was done on the basis of a relative dissolution endpoint (time when 1% of initial scattering intensity remains). The influence of absolute differences in scattering intensity between formulations on data interpretation was minimized by this approach. The applied interpretation is valid under the assumption that a change in scattering intensity during dissolution is dominated by the reduction in particle number. Consideration of particle shrinking or alterations in particle size distribution would require more complex data analysis.

A similar method to assess small particle dissolution was introduced by Tucker *et al.* (34) and Crisp *et al.* (35), who used turbidimetric measurements at an angle of 0° to monitor dissolution of particles with sizes of 0.24–5 μm. An interesting approach was chosen by starting the dissolution process by the addition of surfactants (and a resulting increase in solubility) during the measurement. This procedure enables a determination of the initial absorbance of undissolved particles. Crisp developed a model for the solid mass decay and regarded the particle dissolution process as the shrinking of a sphere. For the case of scattering intensity being proportional to the particle volume he modified his mass decay model towards a turbidity decay model. Both, the dissolution and turbidity based models fit experimental curves well and it is concluded, that "the assumption that turbidity scales as particle volume fraction (concentration) produces reasonable accuracy" (35).

Tucker *et al.* (34) reported dissolution times shorter than 60 s for naproxen nanosuspensions (266 nm and 656 nm; concentration of about 15% of the equilibrium solubility). The same author described that danazol nanosuspensions (Mean 356 nm and 820 nm, 40% of the equilibrium solubility) dissolved in aqueous sodium lauryl sulfate solution in about 150 s. Crisp came to a similar result (< 120 s) for danazol nanosuspensions (D50 300 nm and 400 nm, 10% of the equilibrium solubility) in aqueous sodium lauryl sulfate solution (0.3 wt %) (35). On the other hand the dissolution time for an itraconazole nanosuspension (D50 240 nm, 10% of the equilibrium solubility) was found to be 60 min, which is explained by a lower micellar solubility and a lower rate constant of interfacial reaction for the bigger and more lipophilic itraconazole molecules. The dissolution time for a fenofibrate nanosuspension (D50 130 nm, 40% of solubility S_{NS24h}) of 91 s/101 s (ExpDec1/ExpDec2) stated in this study fits well into the range given by Tucker and Crisp.

In summary we demonstrated that the light scattering method is applicable to measure the dissolution of nanosuspensions. The prefered nanocrystal size is in the lower nanometer range (mean particle size < 500 nm). For very short dissolution times (DT < 1.5 min) the 25 s interval between dilution and first data point might lead to a insufficient number of collected data points, which limits the applicability for extremly rapid processes. In the upper nanometer range (500–1000 nm) it was possible to measure dissolution with the applied setup although the method is less suitable for increasing particle size fractions in the lower micron scale. So far only nanosuspensions, which are used in preformulation studies were investigated. However, in market products the nanosuspensions are usually further processed and more excipients are added to the formulation. A transfer of the scattering dissolution method to later development phases would require an implementation of strategies to cope with undissolvable excipients due to their influence on light scattering measurements. For example prefiltration steps could be included, which we succesfully applied to measure nanocrystal dissolution of a market product (preliminary unpublished data). Finally it should be noted that the measurement of paticle dissolution by light scattering techniques will only allow straightforward data interpretation, if no absorption of light occures at the selected wavelength.

Investigation of Experimentally Obtained Results According to the Noyes-Whitney Equation

The Noyes-Whitney model describes the fundamental principles of diffusion controlled dissolution and has been applied for basic and advanced dissolution modeling

extensively. In this work as a first approach it proved to be useful to check plausibility of experimental data and to gain some mechanistic insight.

By transformation of the Noyes-Whitney equation a linear relation between the dissolution time DT and the term $-\ln(\Delta W/W_S)*V/A_0$ was obtained. The respective diagrams for different concentration gradients displayed a linear graph, despite the fact that nonsink conditions were applied. This observation suggests that the sink classification might be of minor relevance for the dissolution of crystalline nanosuspensions. Their outstanding characteristic, an enhanced surface area, appears to predominate over the influence of concentration gradient in the Noyes-Whitney model. A linear relationship could also be demonstrated for the variation of particle size, despite the assumptions made in the calculation of total initial surface area A_0 and despite the neglect of solubility dependance on particle size.

Dissolution rate constants of $9.4*10^{-4}$ cm/s (variation concentration) and of $5.1*10^{-4}$ cm/s (variation particle size) were calculated from the slopes of the diagrams. We assume that the dissolution rate constant calculated from dissolution of NS 140 nm at different concentrations is more reliable. This presumption is based on the calculation of the surface area under the assumption of spherical particles and the disregard of polydispersity. The error deriving from this is constant for NS140 but varies between different formulations. Nevertheless both values are in a similar range, which means that the dissolution of the investigated system seems to follow a similar mechanism regardless of changes in particle size or concentration. The determined dissolution rate constants fit well into the range given by Crisp, who calculated effective dissolution rate constants of 6–357 $*10^{-4}$ cm/s (35). This comparison confirms that the applied method and data evaluation lead to reliable results. However, for the interpretation of results it is important to mention that neither particle shrinking nor associated changes of effective boundary layer or solubility are considered (28,53). The applied method therefore yields an averaged value for the dissolution rate constant over the entire time of the process.

Shortcomings are associated with the determination of dissolution rate constants in this study and might explain the observed y-offset in our data (Fig. 5 and 6). From the experimental point of view two arguments could be stated. On the one hand for small particle sizes or low concentration gradients the loss of dissolution information during the first 25 s might influence data interpretation essentially. On the other hand for bigger particle sizes the applied data evaluation method has the tendency to underestimate dissolution times as discussed above. From the theoretical point of view the choice of the basic Noyes Whitney dissolution model could be discussed. The Noyes-Whitney equation neither takes into account particle size distributions, nor changes in particle size, surface area, diffusion layer thickness or particle solubility during the dissolution process. For that purposes more complex models of particle dissolution are available (54). Furthermore, the general suitability of diffusion controlled models (like the Noyes-Whitney model) for nanoparticle dissolution has been discussed in literature (35,53). It has been proposed that for nanoparticle dissolution the rate limiting process is not diffusion of dissolved molecule into the bulk solution. Instead the prior solvation step at the solid–liquid interface (the dissociation of drug molecules from the solid) becomes more important for the dissolution process. However, in spite of various simplifications, an approach using the Noyes-Whitney model seems to enable a description of the dissolution process of nanocrystals in a meaningful way.

CONCLUSION

This work focused on the estimation of solubilities and dissolution kinetics of nanocrystalline API by light scattering measurements performed with a Zetasizer Nano ZS™ instrument. In accordance with literature only moderately enhanced solubilities were found, which underlines accelerated dissolution as main factor of the bioavailability enhancement through nanocrystals (5). Manifold shortcomings are associated to conventional and published alternative dissolution methods to assess nanocrystal dissolution. This triggered the development of a method to measure nanocrystal dissolution by monitoring light scattering intensities. The suitability of the experimental setup was demonstrated by direct comparison to a conventional dissolution technique. The new approach was applicable to differentiate between different particle sizes and concentration gradients with a satisfying sensitivity and reproducibility. Operating with volumes as small as few μL of nanosuspensions the presented light scattering method is a small scale approach and could easily be integrated in preformulation studies in early formulation development.

Experimentally determined dissolution times of nanosuspensions showed a linear correlation to concentration gradient and initial particle surface area as predicted by the Noyes-Whitney dissolution model. Despite being designed for constant particle surface area and sink conditions the Noyes-Whitney dissolution model was applicable for a wide concentration range in this study. Evaluation of results on the basis of advanced dissolution models, which consider further parameters relevant for particle dissolution, will help to gain further mechanistic insight from experimental data.

ACKNOWLEDGMENTS AND DISCLOSURES

This work has been supported by the German Federal Ministry of Education and Research in the context of the initiative Spitzencluster—Biotech-Cluster Rhein-Neckar—and the authors thank for funding.

REFERENCES

1. Lipinski CA. Poor aqueous solubility—an industry wide problem in drug discovery. Am Pharm Rev. 2002;5:82–5.
2. Rabinow BE. Nanosuspensions in drug delivery. Nat Rev Drug Discov. 2004;3(9):785–96.
3. Kesisoglou F, Panmai S, Wu Y. Nanosizing–oral formulation development and biopharmaceutical evaluation. Adv Drug Deliv Rev. 2007;59(7):631–44.
4. Muller RH, Gohla S, Keck CM. State of the art of nanocrystals–special features, production, nanotoxicology aspects and intracellular delivery. Eur J Pharm Biopharm. 2011;78(1):1–9.
5. Van Eerdenbrugh B, Vermant J, Martens JA, Froyen L, Humbeeck JV, Van den Mooter G, *et al.* Solubility increases associated with crystalline drug nanoparticles: methodologies and significance. Mol Pharm. 2010;7(5):1858–70.
6. Brunner E. Reaktionsgeschwindigkeit in Heterogenen Systemen. Z Physik Chem. 1904;47(1):56–102.
7. Nernst W. Theorie der Reaktionsgeschwindigkeit in Heterogenen Systemen. Z Physik Chem. 1904;47(1):52–5.
8. Noyes A, Whitney WR. The rate of solution of solid substances in their own solutions. J Am Chem Soc. 1897;19:930–4.
9. Costa P, Sousa Lobo JM. Modeling and comparison of dissolution profiles. Eur J Pharm Sci. 2001;13(2):123–33.
10. Freundlich H. Colloid and capillary chemistry. New York: E. P. Dutton and Company; 1923.
11. Ostwald W. Über die vermeintliche Isomerie des roten und gelben Quecksilberoxyds und die Oberflächenspannung fester Körper. Z Physik Chem. 1900;34:495–503.
12. Kesisoglou F, Wu Y. Understanding the effect of API properties on bioavailability through absorption modeling. AAPS J. 2008;10(4):516–25.
13. Heng D, Cutler DJ, Chan HK, Yun J, Raper JA. What is a suitable dissolution method for drug nanoparticles? Pharm Res. 2008;25(7):1696–701.
14. Xia D, Cui F, Piao H, Cun D, Jiang Y, Ouyang M, *et al.* Effect of crystal size on the *in vitro* dissolution and oral absorption of nitrendipine in rats. Pharm Res. 2010;27(9):1965–76.
15. Shono Y, Jantratid E, Kesisoglou F, Reppas C, Dressman JB. Forecasting *in vivo* oral absorption and food effect of micronized and nanosized aprepitant formulations in humans. Eur J Pharm Biopharm. 2010;76(1):95–104.
16. Jinno J, Kamada N, Miyake M, Yamada K, Mukai T, Odomi M, *et al. In vitro-in vivo* correlation for wet-milled tablet of poorly water-soluble cilostazol. J Control Release. 2008;130(1):29–37.
17. Laaksonen T, Liu P, Rahikkala A, Peltonen L, Kauppinen EI, Hirvonen J, *et al.* Intact nanoparticulate indomethacin in fast-dissolving carrier particles by combined wet milling and aerosol flow reactor methods. Pharm Res. 2011;28(10):2403–11.
18. Li W, Yang Y, Tian Y, Xu X, Chen Y, Mu L, *et al.* Preparation and *in vitro/in vivo* evaluation of revaprazan hydrochloride nanosuspension. Int J Pharm. 2011;408(1–2):157–62.
19. Juenemann D, Jantratid E, Wagner C, Reppas C, Vertzoni M, Dressman JB. Biorelevant *in vitro* dissolution testing of products containing micronized or nanosized fenofibrate with a view to predicting plasma profiles. Eur J Pharm Biopharm. 2011;77(2):257–64.
20. Magenheim B, Levy MY, Benita S. A new *in vitro* technique for the evaluation of drug release profile from colloidal carriers—ultrafiltration technique at low pressure. Int J Pharm. 1993;94(1–3):115–23.
21. Helle A, Hirsjarvi S, Peltonen L, Hirvonen J, Wiedmer SK, Hyotylainen T. Novel, dynamic on-line analytical separation system for dissolution of drugs from poly(lactic acid) nanoparticles. J Pharm Biomed Anal. 2010;51(1):125–30.
22. Bhardwaj U, Burgess DJ. A novel USP apparatus 4 based release testing method for dispersed systems. Int J Pharm. 2010;388(1–2):287–94.
23. Abdel-Mottaleb MM, Lamprecht A. Standardized *in vitro* drug release test for colloidal drug carriers using modified USP dissolution apparatus I. Drug Dev Ind Pharm. 2011;37(2):178–84.
24. Aldridge PK, Melvin DW, Williams BA, Bratin K, Kostek LJ, Sekulic SS. A robotic dissolution system with on-line fiber-optic UV analysis. J Pharm Sci. 1995;84(8):909–14.
25. Chen CS, Brown CW. A drug dissolution monitor employing multiple fiber optic probes and a UV/visible diode array spectrophotometer. Pharm Res. 1994;11(7):979–83.
26. Tsinman K, Avdeef A, Tsinman O, Voloboy D. Powder dissolution method for estimating rotating disk intrinsic dissolution rates of low solubility drugs. Pharm Res. 2009;26(9):2093–100.
27. Alonzo DE, Zhang GG, Zhou D, Gao Y, Taylor LS. Understanding the behavior of amorphous pharmaceutical systems during dissolution. Pharm Res. 2010;27(4):608–18.
28. Galli C. Experimental determination of the diffusion boundary layer width of micron and submicron particles. Int J Pharm. 2006;313(1–2):114–22.
29. Van Eerdenbrugh B, Alonzo DE, Taylor LS. Influence of particle size on the ultraviolet spectrum of particulate-containing solutions: implications for *in-situ* concentration monitoring using UV/Vis fiber-optic probes. Pharm Res. 2011;28(7):1643–52.
30. Mora L, Chumbimuni-Torres KY, Clawson C, Hernandez L, Zhang L, Wang J. Real-time electrochemical monitoring of drug release from therapeutic nanoparticles. J Control Release. 2009;140(1):69–73.
31. Rosenblatt KM, Douroumis D, Bunjes H. Drug release from differently structured monoolein/poloxamer nanodispersions studied with differential pulse polarography and ultrafiltration at low pressure. J Pharm Sci. 2007;96(6):1564–75.
32. Charalampopoulos N, Avgoustakis K, Kontoyannis CG. Differential pulse polarography: a suitable technique for monitoring drug release from polymeric nanoparticle dispersions. Anal Chim Acta. 2003;491:57–62.
33. Kayaert P, Li B, Jimidar I, Rombaut P, Ahssini F, Van den Mooter G. Solution calorimetry as an alternative approach for dissolution testing of nanosuspensions. Eur J Pharm Biopharm. 2010;76(3):507–13.
34. Tucker CJ, inventor. Real time monitoring of small particle dissolution by way of light scattering. United States patent US6750966. 2002.
35. Crisp MT, Tucker CJ, Rogers TL, Williams 3rd RO, Johnston KP. Turbidimetric measurement and prediction of dissolution rates of poorly soluble drug nanocrystals. J Control Release. 2007;117(3):351–9.
36. Chaubal MV, Popescu C. Conversion of nanosuspensions into dry powders by spray drying: a case study. Pharm Res. 2008;25(10):2302–8.
37. van de Hulst HC. Light scattering by small particles. New York: Wiley; 1957.
38. Elsayed MM, Cevc G. Turbidity spectroscopy for characterization of submicroscopic drug carriers, such as nanoparticles and lipid vesicles: size determination. Pharm Res. 28(9):2204-22
39. Hanafy A, Spahn-Langguth H, Vergnault G, Grenier P, Tubic Grozdanis M, Lenhardt T, *et al.* Pharmacokinetic evaluation of oral fenofibrate nanosuspensions and SLN in comparison to conventional suspensions of micronized drug. Adv Drug Deliv Rev. 2007;59(6):419–26.
40. Brittain HG. Particle-size distribution IV. Determination by laser-light scattering. Pharm Technol. 2003;27(10):102–14.
41. Saveyn H, Mermuys D, Thas O, van der Meeren P. Determination of the refractive index of water-dispersible granules for use in laser diffraction experiments. Part Part Syst Char. 2002;19(6):426–32.

42. Lindfors L, Forssen S, Skantze P, Skantze U, Zackrisson A, Olsson U. Amorphous drug nanosuspensions. 2. Experimental determination of bulk monomer concentrations. Langmuir. 2006;22(3):911–6.
43. Chatterjee A, Moulik SP, Sanyal SK, Mishra BK, Puri PM. Thermodynamics of micelle formation of ionic surfactants: a critical assessment for sodium dodecyl sulfate, cetyl pyridinium chloride and dioctyl sulfosuccinate (Na Salt) by microcalorimetric, conductometric, and tensiometric measurements. J Phys Chem B. 2001;105 (51):12823–31.
44. Langguth P, Fricker G, Wunderli-Allenspach H. Biopharmazie. Weinheim: WILEY-VCH Verlag GmbH & Co. KGaA; 2004.
45. Laakso R, Kristoffersson E, Marvola M. Bi-exponential first-order release kinetics of indomethacin from tablets containing polysorbate 80. Int J Pharm. 1984;19(1):35–42.
46. Tinke AP, Vanhoutte K, De Maesschalck R, Verheyen S, De Winter H. A new approach in the prediction of the dissolution behavior of suspended particles by means of their particle size distribution. J Pharm Biomed Anal. 2005;39 (5):900–7.
47. Tay T, Allahham A, Morton DA, Stewart PJ. Understanding improved dissolution of indomethacin through the use of cohesive poorly water-soluble aluminium hydroxide: effects of concentration and particle size distribution. J Pharm Sci. 2011;100(10):4269–80.
48. Sugano K, Okazaki A, Sugimoto S, Tavornvipas S, Omura A, Mano T. Solubility and dissolution profile assessment in drug discovery. Drug Metab Pharmacokinet. 2007;22(4):225–54.
49. Dressman JB, Amidon GL, Reppas C, Shah VP. Dissolution testing as a prognostic tool for oral drug absorption: immediate release dosage forms. Pharm Res. 1998;15(1):11–22. Review.
50. Jamzad S, Fassihi R. Role of surfactant and pH on dissolution properties of fenofibrate and glipizide–a technical note. AAPS PharmSciTech. 2006;7(2):E33.
51. Gao Z. Mathematical modeling of variables involved in dissolution testing. J Pharm Sci. 2011;100(11):4934–42.
52. Dokoumetzidis A, Papadopoulou V, Macheras P. Analysis of dissolution data using modified versions of Noyes-Whitney equation and the Weibull function. Pharm Res. 2006;23(2):256–61.
53. Judefeind A, de Villiers MM. Drug loading into and *in vitro* release from nanosized drug delivery systems. Biotechnol: Pharm Aspects. 2009;10(Nanotechnology in Drug Delivery):129-62.
54. Johnson KC. Comparison of methods for predicting dissolution and the theoretical implications of particle-size-dependent solubility. J Pharm Sci. 2012;101(2):681–9.